Atom Probe Tomography of Compound Semiconductors for Photovoltaic and Light-Emitting Device Applications

Pyuck-Pa Choi,[1] * Oana Cojocaru-Mirédin,[1] Daniel Abou-Ras,[2] Raquel Caballero,[2] Dierk Raabe,[1] Vincent S. Smentkowski,[3] Chan Gyung Park,[4, 5] Gil Ho Gu,[4] Baishakhi Mazumder,[6] Man Hoi Wong,[6] Yan-Ling Hu,[6] Thiago P. Melo,[6] and James S. Speck[6]

[1] Max-Planck-Institut für Eisenforschung GmbH, Max-Planck-Str. 1, D-40237 Düsseldorf, Germany
[2] Helmholtz-Zentrum Berlin für Materialien und Energie, Hahn-Meitner-Platz 1, D-14109 Berlin, Germany
[3] General Electric, Global Research Center, Building K1, 1d41, Niskayuna NY 12309
[4] Dept. of Materials Science and Engineering, Pohang University of Science and Technology (POSTECH), Pohang, South Korea
[5] National Center for Nanomaterials Technology (NCNT), Pohang, Kyungbuk, 790-784, South Korea
[6] University of California, Santa Barbara, CA 93106-5050

* choi@mpie.de

Introduction

Compound semiconductors belong to the most important materials for optoelectronic applications [1–4]. Many of them exhibit favorable optical properties, such as a direct energy band gap (in contrast to silicon) and high-absorption coefficients over a wide spectral range [5]. Moreover, varying the composition of the compound or substituting some of its elements often allows for controlled band gap engineering and optimization for specific applications. Because many compound semiconductors enable efficient conversion of light into electricity and vice versa, they are commonly used materials for optoelectronic devices.

A full understanding of the properties of compound semiconductor devices requires quantitative compositional analyses at spatial resolutions finer than the nanometer scale. In the past decade, atom probe tomography (APT) has emerged as one of the most powerful techniques for mapping the elemental distribution in semiconductors spatially with near-atomic resolution [6]. The present article highlights recent APT results on some of the most prominent compound semiconductors for photovoltaic ($Cu(In,Ga)Se_2$ [1, 2] and CdTe [3]) and light-emitting device (group III-nitrides [4]) applications. It will be demonstrated that APT can provide a profound understanding of these compound semiconductor materials/devices by giving new insights into the atomic-scale elemental distribution.

Methods and Materials

The optoelectronic devices presented in this paper comprise thin layers with thicknesses in the nanometer to micrometer range, and the details specific to each specimen are given below. The complex device structures and the limited size of the volume probed by APT (typically $100 \times 100 \times 500\ nm^3$) make the preparation of APT samples very challenging. In order to place the region of interest (for example, the active layers) within the analyzed volume, focused-ion-beam (FIB) milling is employed. Site-specific APT sample preparation methods based on FIB involve several steps. First, rectangular trenches are milled into the device leaving behind a lamellar or wedge-shaped piece of the sample containing the region of interest (for example, the active layers). Subsequently, this piece is lifted out using a micro-manipulator and attached to support tips. Finally, annular FIB milling is performed to prepare fine, needle-shaped APT samples with a typical radius of curvature of 100 nm or below. A detailed description of the preparation of APT samples using FIB can be found in [7].

Results

CIGS thin-film solar cells. $Cu(In,Ga)Se_2$ (CIGS) solar cells were fabricated at the Helmholtz-Zentrum Berlin für Materialien und Energie. Details about CIGS deposition and cell stacking are given elsewhere [8]. APT samples were prepared by means of focused-ion-beam (FIB) milling according to the standard procedures described in [7]. We found that choosing low specimen temperatures, laser pulse energies, and pulse repetition frequencies yields the best agreement with the overall compositions measured by other techniques, such as secondary ion mass spectrometry and X-ray fluorescence.

Figure 1 shows three-dimensional (3D) elemental maps of the Cu and In matrix elements as well as Na and K impurities at a grain boundary (GB). These impurities originate from the soda lime glass (SLG) substrate, which contains significant amounts of Na_2O and K_2O. It can be seen that both Na and K atoms are highly enriched in a two-dimensional (2D) zone. In conjunction with complementary transmission electron microscopy (TEM) studies (not presented here), the region exhibiting enhanced Na and K concentrations was identified as a high-angle GB. The apparent width of the GB segregation zone (about 4 nm) is substantially larger than the typical structural width of a GB (about 1 nm). Such a discrepancy can be partly ascribed to a local magnification effect [9] in APT. The measured bulk compositions of the neighboring grains are slightly different, with In and Cu concentrations slightly varying from one grain to the other. While Na and K impurities are enriched at the GB, their concentrations inside the CIGS grains are highly dilute, amounting to about 200 ppm for Na and 90 ppm for K. Na is in higher concentration at the GB (about 3.5 at.%) than K (about 0.3 at.%), which can

 doi:10.1017/S1551929512000235

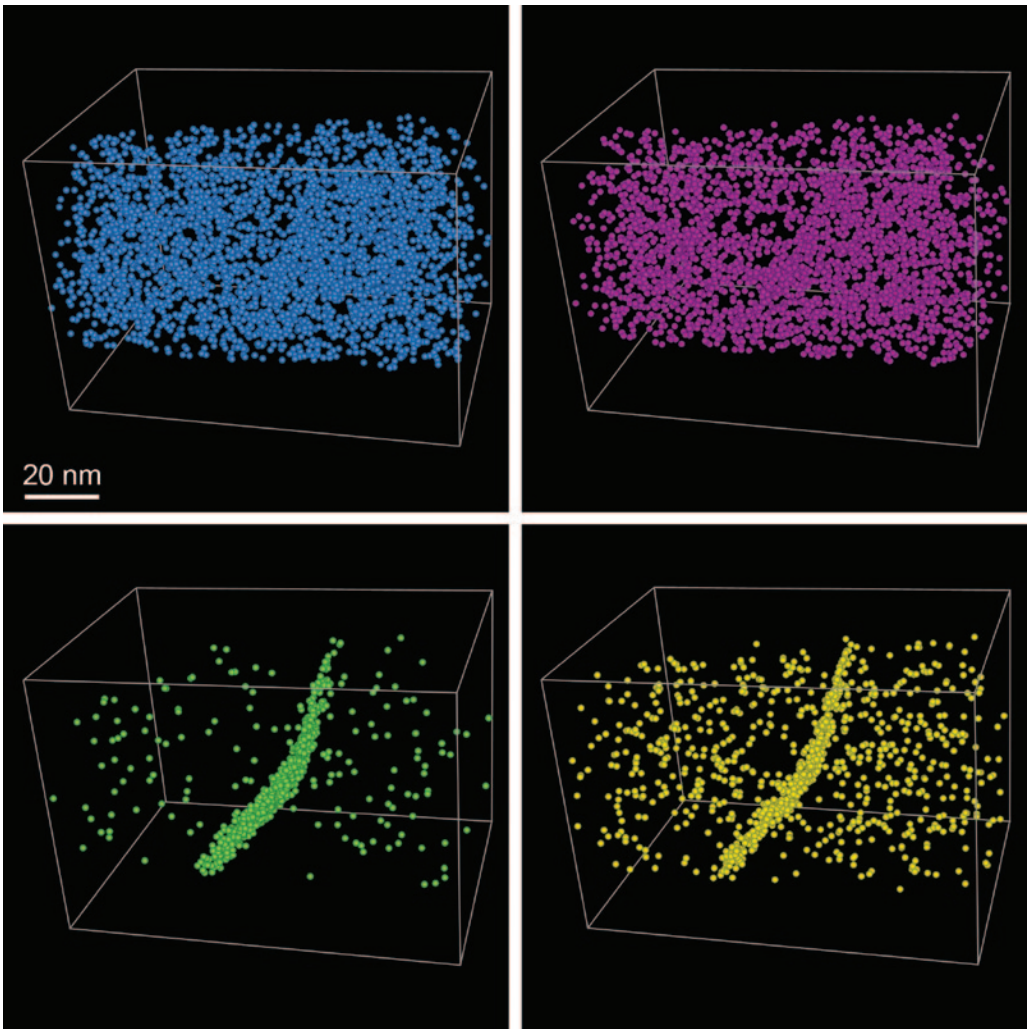

Figure 1: 3D atom maps of a solar-grade $Cu(In,Ga)Se_2$ thin film. On the left are matrix atoms Cu (blue) and In (magenta), and on the right are impurity atoms Na (green) and K (gold).

be explained by a higher content of Na in the SLG substrate, as well as a higher diffusivity due to a smaller ionic radius as compared with K. Furthermore, the Na and K segregation at the GB is accompanied by Cu depletion and In enrichment, which is indicative of Na_{Cu} and K_{Cu} defects at the GB. The exact mechanisms leading to such compositional variations at the CIGS GB are still under investigation. They are probably related to atomic or ionic redistribution processes occurring during CIGS deposition, which reduce the GB charge and the overall GB energy. We also found that the GB composition can strongly vary depending on the GB character and orientation. Systematic APT studies, in conjunction with complementary techniques, are required to understand the compositional variations at CIGS GBs and their effect on the electrical properties of solar-grade CIGS films.

To our knowledge, APT is currently the only technique capable of tracing compositional changes for both matrix and impurity elements at CIGS grain boundaries. Because of the high signal-to-noise ratio, even highly dilute impurity concentrations in the tens of ppm range can be detected. Because APT enables 3D elemental mapping with sub-nanometer resolution, GBs "buried" under the surface can be resolved. Another advantage of the APT technique is that the detection sensitivity is not element-specific if appropriate measurement parameters are selected.

It should be noted that impurities may not only affect the electrical properties of GBs but also other parts of the solar cell (for example, the p-n junction or the back-contact region, etc.). Systematic APT studies of CIGS thin-film solar cells are important for understanding their complex underlying physics, and active research in this field is just at its beginning [10, 11].

CdTe thin-film solar cells. The first APT data collected from a CdTe layer within a CdTe solar cell prepared with standard $CdCl_2$ and Cu treatments [12] are reported here. Standard site-specific FIB lift-out techniques [8] were used to prepare specimens from a typical CdTe layer in a solar cell. The top surface of the as-received specimen had significant roughness. Hence, the top 50 nm of CdTe was removed and not sampled by APT. The total depth analyzed by APT was about 530 nm. The data were collected on a Cameca Instruments, Inc. LEAP™ 4000 X HR operated at a temperature of 40 K in laser pulsing mode.

Figure 2 reveals the mass spectrum generated from the APT analysis, which is one of the most complex APT spectra published to date. In addition to detecting the elements of interest, the spectrum reveals a large number of molecular ions. It is important to stress that spectra with this level of complexity require the use of instruments with high mass resolution in order to minimize peak overlap. Commercially available algorithms can then be used to provide quantitative analysis of these complex APT spectra, as we will show below. Although the APT spectra are complex, there is a lot of redundancy in the spectra. For the example shown here, all of the isotopes of Cd, Te, as well as Cd_xTe_y-based molecular ions, are detected. Keenan et al. [13] have recently demonstrated that multivariate statistical analysis (MVSA) algorithms can be used to reduce the redundancy in the measured data and thereby distill the massive amount of chemical information into a handful of chemical components that fully describe the data set in an unbiased fashion. Each MVSA component has two contributions, a 2D or 3D map (revealing the locations of species) and an

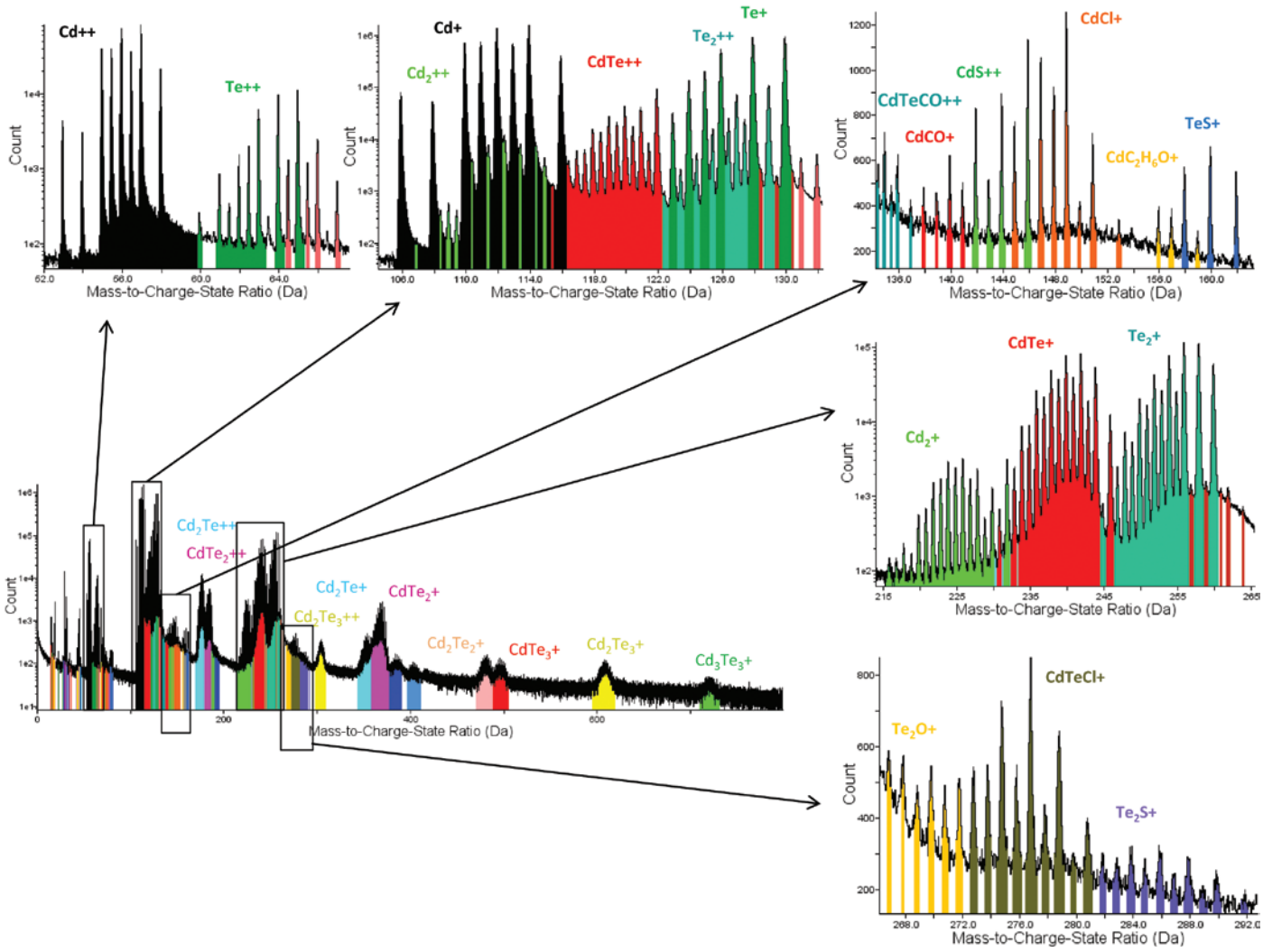

Figure 2: Mass spectrum acquired from the APT analysis of a solar-grade CdTe film. In addition to detecting the elements of interest, the spectrum reveals a large number of molecular ions.

associated spectrum (identifying the compositions of the species present in the 2D or 3D map).

Figure 3a shows 3D maps of Cl, S, CdS, CdCl, TeS, and a color overlay of CdCl (orange), Cd (black), and Te (dark green) in the top-left corner. The top panel of Figure 3b reveals a 2D (X-Y) slice through the 100-nm-thick region indicated by the dashed black box in Figure 3a. These maps show enrichment of S and Cl at the grain boundary. An advantage of APT is that the signal is inherently quantitative for *both* the matrix composition and the trace species present at grain boundaries. The bottom panel of Figure 3b shows concentration depth profiles of selected elements (Cd, Te, S, Cl) along a region of interest (marked by the blue box).

InGaN/GaN multiple quantum wells. InGaN/GaN multiple quantum wells (MQWs) are commonly used as active layers in light-emitting diodes (LEDs) and laser diodes (LDs) [14]. The properties of InGaN-based optoelectronic devices are essentially controlled by the atomic-scale composition and interfaces [15] of the MQWs. Accordingly, APT studies of InGaN/GaN MQWs are essential for understanding InGaN-based LEDs and LDs. The occurrence of In fluctuation or In clustering is still debated because of the extreme sensitivity of InGaN layers under high electron beam doses during TEM analysis [16]. APT provides information on both the composition and size of the clusters with near-atomic resolution and is therefore a powerful tool for studying such compositional fluctuations.

APT analyses were carried out using a laser-assisted wide-angle tomographic atom probe (CAMECA-LAWATAP™, Cameca Instruments). TEM specimens and needle-shaped APT samples with a radius of curvature less than 50 nm (Figure 3a) were prepared by means of a standard protocol [8].

Figure 4a shows an elemental map acquired from the APT analysis of an LED device from p-GaN to n-GaN. Figure 4b shows the In maps of individual quantum wells (region "a" and "b" in Figure 4a) and the corresponding concentration maps of In, which are color-coded. Using such concentration maps, the homogeneity of the In distribution within the layers can be studied. The lateral distribution of In atoms in the InGaN quantum well layers is inhomogeneous (see Figure 4b), though the composition of the InGaN layers along the *z*-direction is uniform. These results reveal that the InGaN layers studied

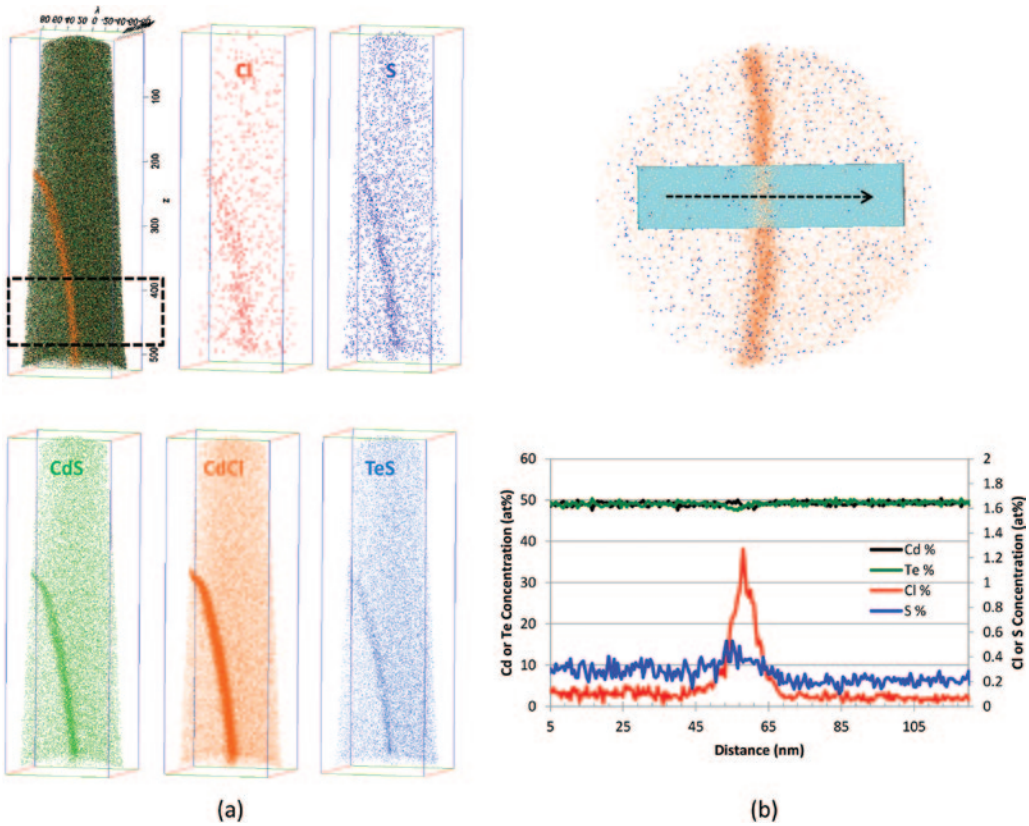

Figure 3: 3D atom maps of a solar-grade CdTe thin film. (a) 3D maps showing the distribution of Cl (red), S (dark blue), CdS (green), CdCl (orange), and TeS (light blue). (b) 2D elemental map constructed from the volume indicated in the dashed black box in (Figure 3a), and 1D composition profiles along the rectangle in the top panel of Figure 3b.

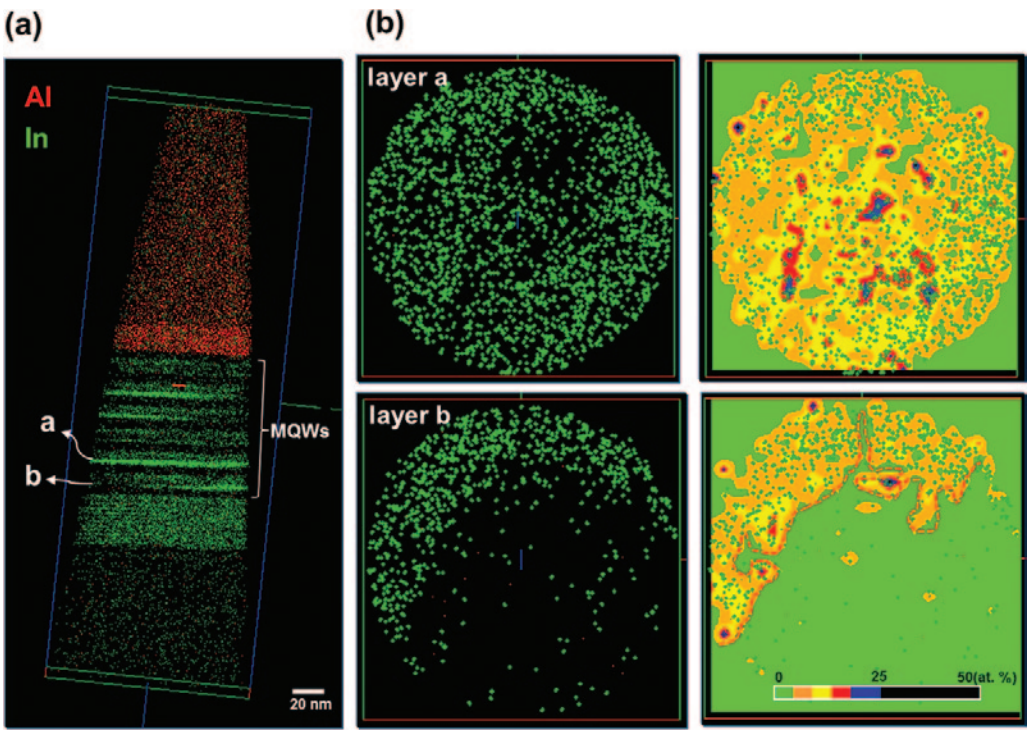

Figure 4: 3D atom maps of active layers in an LED. (a) 3D atom map of LED device from p-GaN to n-GaN. The red and green dots represent Al and In atoms, respectively. For clarity, the other elements are not shown. (b) In maps of individual quantum wells (layer a and b as marked by arrows in Figure 4a) and corresponding In concentration maps, which are color-coded for concentration level.

in this work exhibit intrinsic compositional fluctuations.

The root mean square (RMS) roughness of the InGaN layers as a function of the position from the n-GaN substrate was also measured. The RMS roughness of the upper interfaces is higher than that of the lower interfaces. These characteristics of the interface roughness are important because the recombination of electrons and holes mainly occurs at the first InGaN layer near the p-GaN substrate.

N-face and Ga-face GaN/AlN heterostructure. The group III nitrides commonly form in their lowest free-energy wurtzite structure (space group $P6_3mc$, point group 6mm) and are polar along the *c*-axis. Current work in optoelectronic devices such as LEDs and LDs is focused on avoiding the deleterious effects of polarization-related electric fields while electronic devices benefit from the high, fixed polarization-related sheet charges at heterointerfaces. APT studies of GaN-based materials can provide answers to important questions related to the elemental distribution at or below the nanoscale.

GaN/AlN samples were grown in a Varian Gen-II Plasma-Assisted Molecular Beam Epitaxy (PAMBE) system under metal-rich conditions [17]. For this study a CAMECA LEAP 3000 X HR was used. Figure 5a illustrates the 3D atom distributions in an N-face GaN multilayered structure. The first two layers (light blue at z = 80 nm and z = 100 nm) are nominally pure AlN, grown by the N-rich and metal-rich method, respectively. For a detailed analysis of the interfaces, a cylindrical volume of 20 nm in diameter and 30 nm in length was selected from the center data set to avoid any

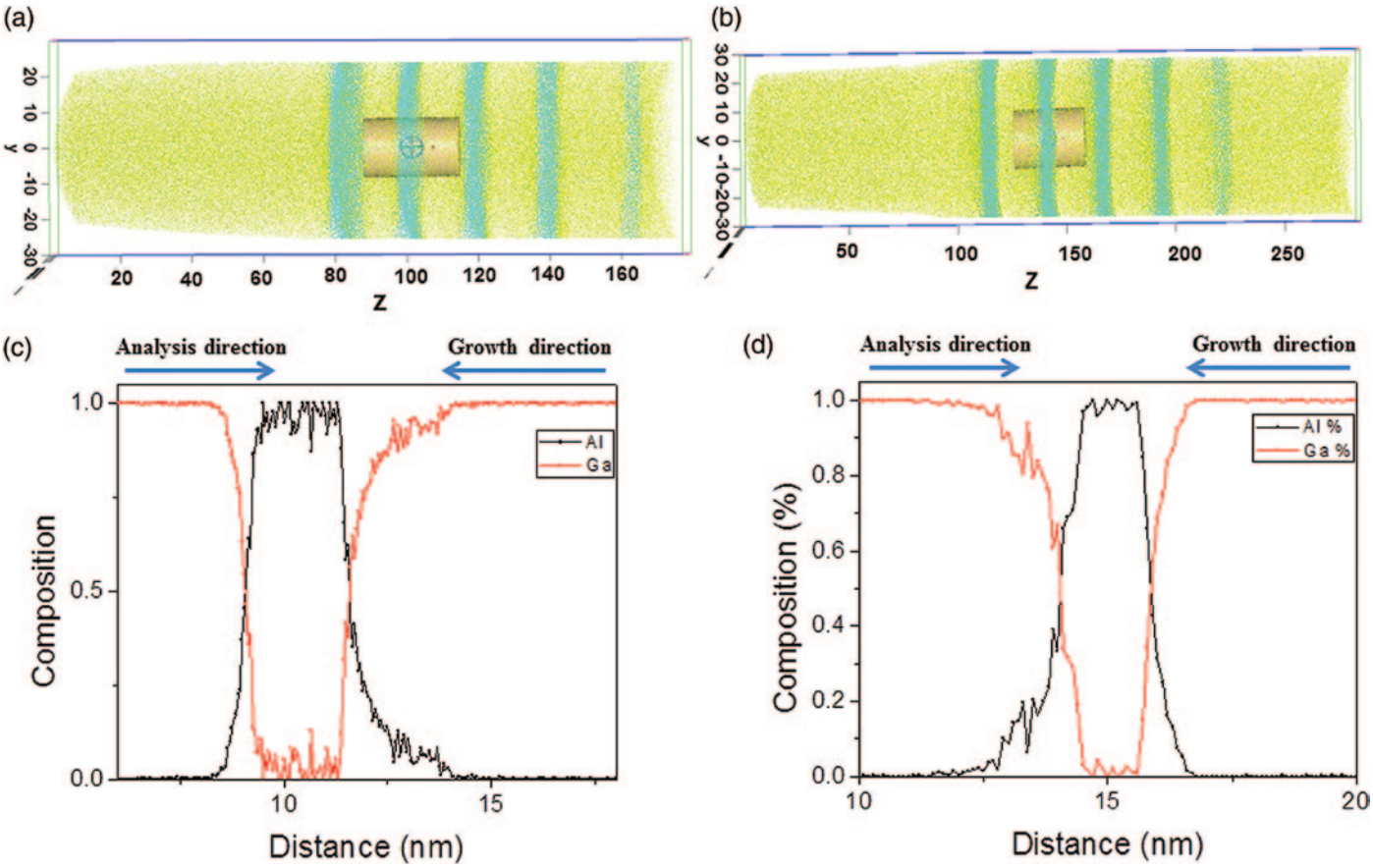

Figure 5: 3D atom maps of GaN/AlN heterostructures. (a) and (b) 3D maps showing the distribution of Al (light blue), Ga (yellow), and N (green) in an N-face GaN/AlN and a Ga-face GaN/AlN heterostructure. (c) and (d) show the 1D compositional profile along the cylinders (20 × 20 × 30 nm^3) in Figure 5a and 5b, respectively.

concave interfaces resulting from limitations in the reconstruction algorithm. Figure 5c depicts one-dimensional (1D) compositional profiles of Ga and Al along the tip direction revealing the nature of interfaces between AlN and GaN. It was found that the top interface (between AlN and GaN grown on top) and bottom interface (between GaN and AlN grown on top) are asymmetric and that the top interface was more abrupt than the bottom one. The measured RMS roughness values of the top and bottom interfaces are 0.323 nm and 0.428 nm, respectively.

Figure 5b shows a similar multilayer structure on a Ga-face GaN substrate. The corresponding concentration depth profiles of Al and Ga are presented in Figure 5d. Apart from being asymmetric, the two interfaces exhibited a reversed behavior from the N-face multilayers. The RMS roughness values of the top and bottom interfaces in this case are 0.468 nm and 0.302 nm. These data reveal that the structural and compositional characteristics of the GaN/AlN/GaN interfaces depend on the sense of the polarity at the interface. The diffuse interfaces are not caused by the metal-rich growth process (plasma-assisted multiple beam epitaxy or PAMBE) because the N-rich AlN layer exhibits similar behavior but are probably associated with the negative polarization charge.

Conclusions

We have presented atom probe tomography (APT) results on technologically important compound semiconductor materials for photovoltaic and LED applications. APT can provide atomic-scale insights about the active layers of optoelectronic devices and information on the spatial distribution of matrix as well as impurity elements. Thus, APT, in conjunction with complementary techniques such as TEM, is a powerful tool for elucidating the structure-property relationships of optoelectronic devices. APT research on compound semiconductors is expected to expand rapidly in the upcoming years and will contribute significantly to understanding of the complex defect physics of compound semiconductors.

References

[1] S Scheer and HW Schock, *Chalcogenide Solar Cells*, WILEY-VCH, Weinheim, 2011.

[2] WN Shafarman and L Stolt, "Cu(In,Ga)Se2 solar cells" in *Handbook of Photovoltaic Science and Engineering*, eds. A Luque and S Hegedus, John Wiley & Sons, 2003, West Sussex, England, 567–616.

[3] BE McCandless and JR Sites, "Cadium telluride solar cells" in *Handbook of Photovoltaic Science and Engineering*, eds. A Luque and S Hegedus, John Wiley & Sons, 2003, West Sussex, England, 617–62.

[4] EF Schubert, *Light-Emitting Diodes,* Cambridge University Press, Cambridge, UK, 2010.

[5] AM Barnett and A Rothwarf, *IEEE T Electron D* 27 (1980) 615–30.

[6] TF Kelly, DJ Larson, K Thompson, RL Alvis, JH Bunton, JD Olson, and BP Gorman, *Annu Rev Mater Res* 37 (2007) 681–727.
[7] MK Miller, KF Russell, K Thompson, R Alvis, and DJ Larson, *Microsc Microanal* 13 (2007) 428–36.
[8] CA Kaufmann, R Caballero, T Unold, R Hesse, R Klenk, S Schorr, M Nichterwitz, and HW Schock, *Sol Energ Mat Sol C* 93 (2009) 859–63.
[9] MK Miller and MG Hetherington, *Surf Sci* 246 (1991) 442–49.
[10] E Cadel, N Barreau, J Kessler, and P Pareige, *Acta Mater* 58 (2010) 2634–37.
[11] O Cojocaru-Mirédin, P Choi, R Wuerz, and D Raabe, *Ultramicroscopy* 111 (2011) 552–56.
[12] NR Paudel, D Kwon, M Young, KA Wieland, S Asher, and AD Compaan, *35th IEEE PVSC* (2010) 1009–13.
[13] MR Keenan, VS Smentkowski, RM Ulfig, E Oltman, DJ Larson, and TF Kelly, *Microsc Microanal* 17 (2011) 418–30.
[14] S Nakamura, *Science* 281 (1998) 956–61.
[15] YC Cheng, EC Lin, CM Wu, CC Yang, JR Yang, A Rosenauer, KJ Ma, SC Shi, LC Chen, and CC Pan, *Appl Phys Lett* 84 (2004) 2506–08.
[16] TM Smeeton, MJ Kappers, JS Barnard, ME Vickers, and CJ Humphreys, *Appl Phys Lett* 83 (2003) 5419–21.
[17] B Heying, R Averbeck, LF Chen, E Haus, H Riechert, and JS Speck, *J Appl Phys* 88 (2000) 1855–60.

MT